International Journal of Heat and Mass Transfer 52 (2009) 2992–2999

Contents lists available at ScienceDirect

International Journal of Heat and Mass Transfer

journal homepage: www.elsevier.com/locate/ijhmt

Electroosmotic flow in sludge flocs

Z. Yang [a], X.F. Peng [a,*], D.J. Lee [b]

[a] Laboratory of Phase Change and Interfacial Transport Phenomena, Department of Thermal Engineering, Tsinghua University, Beijing 100084, China
[b] Department of Chemical Engineering, Taiwan University, Taipei 106, China

ARTICLE INFO

Article history:
Received 18 November 2008
Received in revised form 6 January 2009
Accepted 10 February 2009
Available online 28 March 2009

Keywords:
Electroosmotic flow
Sludge floc
Flow distribution
Permeability

ABSTRACT

Electroosmotic flow in sludge flocs is one of important transport processes playing a critical role in electroosmotic dewatering of sludge. In the present work both fluorescence in situ hybridization (FISH) and confocal laser scanning microscope (CLSM) are employed to obtain the interior structural information of flocs and the structural properties are incorporated into the computation of electroosmotic flow inside flocs. Some important parameters, including flowrate distribution, pressure drop and permeability, were specifically investigated to explore the flow characteristics. An investigation was also conducted to compare the electroosmotic flow with the corresponding pressure driven flow inside flocs.

1. Introduction

Electroosmotic flow or electroosmosis is induced by the interaction between an external electrical field and the boundary region of a polar liquid in a flow passage or channel. Due to special electrochemical reactions, a so-called electrical double layer (EDL) forms on solid–liquid interface and constitutes an ionized mobile region on the liquid side. As subject to an external electrical field applied along the channel, the ionized mobile liquid region is forced into flowing and subsequently drives the neutral liquid in the central channel via the molecular viscosity. In this way, an electroosmotic flow occurs. Usually, in a macro-scaled channel the ratio of channel diameter/width to the EDL width, typically of dozens of nanometers, is very large and electroosmotic flow, if there is, is so weak that can be safely neglected as compared with pressure driven flow [1]. As the scale goes down to micrometer, the viscous effect of liquid becomes significant and begins to suppress pressure driven flow, and consequently, electroosmotic flow becomes relatively important, or even dominant under some conditions.

Using electroosmotic flow to propel liquid in micro-structures becomes appealing due to several unique advantages. First, it can effectively produce liquid flow in channels at a scale of micrometer or smaller, which is quite difficult in a pressure driven flow due to the requirement of a high pressure gradient. Second, it possesses good controllability on flow mode through easily adjusting the external electrical field. For instance, Oddy et al. [2] applied an alternating electrical field to change the electroosmotic flow in a $100 \times 40\ \mu m^2$ channel so as to efficiently mix different liquids.

Electroosmotic dewatering of sludge, i.e., applying electroosmotic flow to dewater sludge, have become an applicable novel technology in waste water treatment industry and other drying processes. Before its further disposal, the byproduct of waste water treatment – sludge should be well dewatered to reduce its volume and mass to save the treatment cost. Compared with traditional dewatering treatments, such as naturally freeze–thaw [3,4] and heating, electroosmotic dewatering of sludge can speed up treatment rate, reduce energy consumption in post-processing [5] and save as much as 17.4–25.6% of treatment cost [6]. Being dominated by complicated electrical, physical and chemical mechanisms, electroosmotic dewatering of sludge shows many special phenomena. The most prominent one is the structural variation of sludge during the dewatering process [7,8]. Another one is that the way in which structure morphology of sludge changes during dewatering closely depends on the position inside sludge, because anode and cathode play distinct roles in electroosmosis [9]. Also, distribution of water content, though being a result of electroosmotic dewatering, can effectively change the dewatering process [10–12].

Since sludge is composed of flocs, electroosmotic dewatering of sludge is mainly determined by water flow in the inner structure of flocs. Hence, a comprehensive investigation of electroosmotic flow of water inside flocs is quite necessary for the understanding of electroosmotic dewatering of sludge. Generally, flocs are treated as a type of porous media with 60–99% of their volume occupied

* Corresponding author. Tel./fax: +86 10 6278 9751.
E-mail address: pxf-dte@mail.tsinghua.edu.cn (X.F. Peng).

0017-9310/$ - see front matter © 2009 Elsevier Ltd. All rights reserved.
doi:10.1016/j.ijheatmasstransfer.2009.02.022

Nomenclature

A_{pore}	pore area (m^2)
D_{pore}	diameter of pore (m)
E	electric intensity (V/m)
$\vec{i}$	vector unit in x-direction (−)
$\vec{j}$	vector unit in y-direction (−)
$\vec{k}$	vector unit in z-direction (−)
K_p	permeability of pressure driven flow (m^2)
K_{EM}	permeability of electroosmotic flow (C/m)
l_x	length of floc in the x-direction (m)
l_y	length of floc in the y-direction (m)
l_z	length of floc in the z-direction (m)
p	pressure (Pa)
u	velocity in the x-direction (m/s)
v	velocity in the y-direction (m/s)
w	velocity in the z-direction (m/s)

Greeks

ε_0	vacuum permittivity, 8.854×10^{-12} (F/m)
ε	relative permittivity, 80 for water (−)
ζ_w	surface zeta potential of floc (V)
μ	water viscosity, 1.003×10^{-3} ($kg \cdot m^{-1} \cdot s^{-1}$)
ρ	water density, 1000 ($kg\ m^{-3}$)

by water. The typical pore size inside flocs is about tens of micrometers, a right scale at which electroosmotic flow becomes important.

This paper is dedicated to study electroosmotic flow in flocs. First the inner structures of several sludge samples were obtained by carrying out CLMS experiments and a series of image processing steps. Secondly, a CFD simulation model was established to investigate the inside-floc water flow. And finally, the numerical data were acquired and processed. The work here incorporated the complicated interior structural properties of flocs into the investigation of flow characteristics and considered the detailed characteristics of electroosmotic flow, which was rarely done before in the open literature.

2. Samples and computational meshes

2.1. Samples

Waste-activated sludge was taken from the Min-Sheng Municipal Wastewater Treatment Plant in Taipei, which was gravitationally settled to a solid content of around 15,000 mg/L and was the testing sample for the present work. The chemical oxygen demand (COD) for the sludge was 24,400 mg/L, obtained from direct reading spectrometer (DR = 2000, HACH, Loveland, CO, USA). The density of dry sludge was measured by an Accupyc Pycnometer 1330 (Micromeritics, Norcross, GA, USA) as 1450 kg/m^3. Three flocs samples were acquired from the waste-activated sludge and denoted hereafter as floc A, B and C.

2.2. FISH and CLSM

The CLSM (OLYMPUS BX50) equipped with an image processor (OLYMPUS FV5 PSU) and an argon laser source was adopted to stimulate the fluorescence. The sludge floc was imaged with a 10× objective with the software FLUOVIEW version 3.0. The microscope scanned the samples at a specified depth and digitized the image obtained. Sludge flocs for CLSM analysis were first fixed with 3% paraformaldehyde in phosphate-buffered saline (PBS). Then the fixed sample was embedded in low-melting-point agar (with melting point of 75 °C and gelling point of 38 °C) for the FISH. In this study, the probes, EUB338 (labeled by rhodamine) and ARCH915 (labeled by tetrachlorofluorescein) were employed for detecting of members of domain Bacteria with high cellular ribosome content and those that cannot be detected by EUB338. The stained samples were washed three times to remove extra probes by hybridization buffer solution.

2.3. Floc image and 3D structures

More than 100 CLMS images were taken for a floc sample, and the image-thresholding algorithm (Otsu's method [13]) was used to determine the thresholding value of each sliced image. Using the thresholding value, these images were converted and turned into white-black images. Next, the three-dimensional image for the floc was reconstructed using the converted CLSM images. Then, the software Amira 3.0 (TGS Inc., Hudson, NH, USA) was used to reconstruct the thresholded sliced images as isosurfaces (polygonal surface models and volumetric grids). The reconstruction procedures basically followed those in the investigation of Chu and Lee [14,15] and detailed procedures were listed in Ref. [16]. Fig. 1 shows one typical CLMS slice-cut of the floc sample A, its converted image (solid in white and pore in black), the 3D CLMS image and the reconstructed 3D floc mesh for computation. The geometric properties of the three floc samples are listed in Table 1. Detailed analysis on the floc structure can be found in Ref. [17].

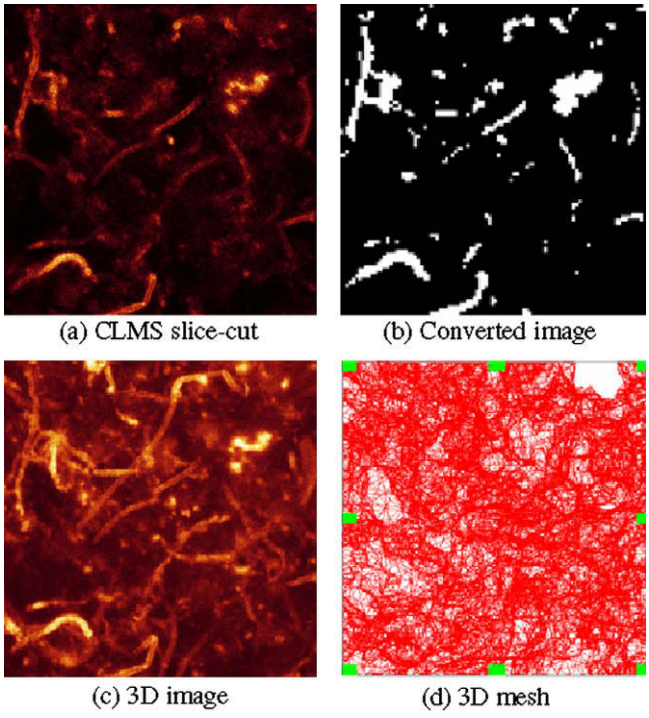

Fig. 1. Floc image and 3D structure.

Table 1
Geometric property of the floc samples.

Floc sample	Size/μm	Porosity	Grid number in pore
A	113 × 113 × 107	0.628	76,720
B	94 × 94 × 94	0.615	74,179
C	78 × 78 × 115	0.629	49,821

3. Numerical modeling

3.1. Computational meshes

Meshes like that in Fig. 1(d) were imported into FLUENT 6.0 to further compute fluid flow inside the floc samples. The computational domain covered the whole pore space inside the flocs which was a collection of all the mutually-intersecting channels. One face of the floc cube was assigned as the flow inlet and the other one on the opposite side as the outlet. The remaining four side faces were treated as impermeable walls. Assuming impermeable side walls can keep a conservative water flowrate on any cross-section from the inlet to the outlet. If the side walls are permeable, water may flow out of or into the floc, causing a changing flowrate along the flow direction, as shown in the case of a spherical floc with its entire spherical surface being permeable in Ref. [18]. The dependence of computation on grid mesh was checked by studying the permeability of a series of meshes for the same floc structure while with different grid numbers. When the value of the permeability became steady, judged by the criterion that its change was no more than 3% as grid number of current mesh reduced to 50% of the previous one, the current mesh was regarded as a proper mesh with good computational confidence. Grid numbers for the final meshes adopted in this work are listed in Table 1.

3.2. Governing equations

For the water flow in the pores of a floc, steady impressible Newtown fluid laminar equations hold

$$\nabla' u' = 0 \tag{1}$$

$$\left(\vec{u}' \cdot \nabla'\right) u' + \nabla' p' = \frac{1}{Re} \nabla^2 \vec{u}' \tag{2}$$

and

$$\vec{u}' = \frac{\vec{u}}{u_w}, \quad p' = \frac{p}{\rho u_w^2}, \quad x' = \frac{x}{l_m}, \quad y' = \frac{y}{l_m}, \quad z' = \frac{z}{l_m}, \qquad \nabla' = \frac{\partial}{\partial x'}\vec{i} + \frac{\partial}{\partial y'}\vec{j} + \frac{\partial}{\partial z'}\vec{k} \tag{3}$$

where $\vec{u} = u\vec{i} + v\vec{j} + w\vec{k}$. u_w is the characteristic velocity of electroosmotic flow which will be discussed in the later section. l_m is the characteristic length of the floc defined as the geometric average of the three edges of the floc cube, i.e., $l_m = (l_x l_y l_z)^{1/3}$.

The boundary conditions for Eqs. (1) and (2) are as follows.

a) on the surface of the floc

$$\vec{u}' = \vec{e}_t \cdot \sin\alpha \tag{4a}$$

b) at the inlet

$$v' = 0, \quad w' = 0, \quad p' = 0 \tag{4b}$$

c) at the outlet

$$p' = 0 \tag{4c}$$

where $\vec{e}_t$ is the unit vector of electric intensity, α the angle between $\vec{e}_t$ and the local surface normal. The Reynolds number Re in Eq. (2) is defined as

$$Re = \frac{\rho u_w l_m}{\mu} \tag{5}$$

and u_w is

$$u_w = -\frac{\varepsilon\varepsilon_0\zeta_w}{\mu} E \tag{6}$$

where ζ_w is the zeta potential on the surface of floc and has a value of -0.0225 V for the floc samples studied here. Eq. (6) is the so-called Smoluchowski equation, valid on the equilibrium between the electrical force and the viscous force in the boundary region. Using the Smoluchowski equation to account for the electroosmotic flow on the boundary needs to meet one specific requirement that the size of the channel should be significantly larger than the EDL thickness. According to the analysis on flow resistance in the previous investigation [1], as the ratio of the channel width to the EDL thickness surpasses 50, electroosmotic flow can be hydrodynamically treated as a normal pressure driven flow with an electroosmotic sliding boundary condition, or in another word, the Smoluchowski equation can be safely applied. Considering that the typical EDL thickness ranges from 1 to 100 nm, the channel width that makes the Smoluchowski equation valid, by a conservative estimation, is above 50 times of the super limit of the EDL width, i.e., 5 μm. For a typical cross-section of floc A, as shown in Fig. 1(b), its pore-size distribution is shown in Fig. 2. The curve represents the pore area differential, dA_{pore}/dD_{pore}, changing with the pore diameter, D_{pore}. So the area under the curve, i.e., the accumulation, is right the pore area. Very clearly, pores with diameter lager than 5 μm, where the Smoluchowski equation can be safely applied to study the electroosmotic flow, have an accumulated area (the grayed part in Fig. 2) exceeding 95% of the total pore area (the whole area under the curve). As a result, assuming the electroosmotic flow with Smoluchowski boundary in all pores should have an error less than 5%.

In addition to the channel width, the ratio of dielectric constants between the fluid and solid can also influence the electroosmotic flow via changing the electric streamlines in porous media [19]. In this study, the ratio of dielectric constants is assumed to be one, so that the electric streamlines regress into a set of uniformly distributed straight lines along the flow direction in the floc, resulting in $\vec{e}_t$ in Eq. (4a) pointing from the inlet to the outlet anywhere insider the floc, which greatly simplifies the calculation, however, still keeps the most interesting features of electroosmotic flow.

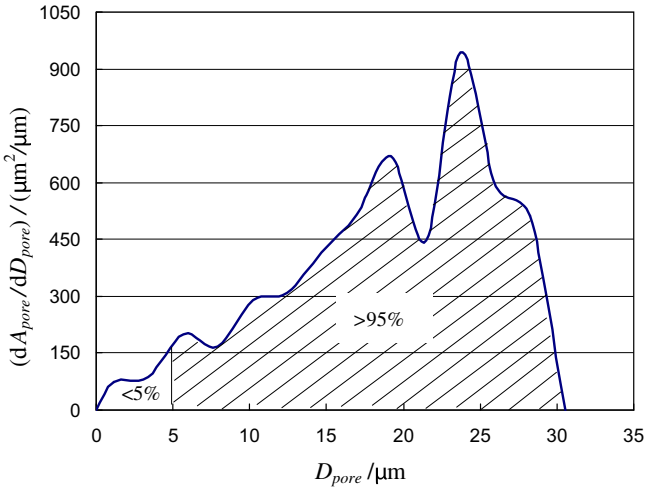

Fig. 2. Distribution of pore area A_{pore} in Fig. 1b.

For a comparative study, flow driven by pressure gradient in flocs without electroosmotic force is also considered, denoted here as pressure driven flow. The governing equations for the pressure driven flow in pores are exactly the same as Eqs. (1) and (2), except that the boundary conditions are specified as follows.

a) on the floc surface

$$\vec{u}' = 0 \tag{7a}$$

b) at the inlet

$$u' = 1, \quad v' = 0, \quad w' = 0 \tag{7b}$$

c) at the outlet

$$p' = 0 \tag{7c}$$

It should be noted that the characteristic velocity here used to normalize velocities in Eqs. (1) and (2) is the mean velocity, u_m. Introducing u_m, instead of u_w, can facilitate the analysis of the size influence on floc permeability, which will be addressed later.

Eqs. (1)–(7) are solved in FLUNET 6.0. The computational domain was discretized into finite volumes using tetrahedral grids. All variables were stored in the centers of grids. A second-order upwind scheme was used for the convective fluxes, and a central-differencing scheme was used for discretizing the diffusion fluxes. The pressure–velocity coupling method was SIMPLE algorithm. The criterion for terminating the iteration was that all the dimensionless residuals for all equations drop below 10^{-4}.

4. Flow behavior

4.1. Flow distribution

Flow distribution is mainly determined by the flow driving mechanism. In a pressure driven flow, fluid flow is severely suppressed near the boundary due to the strong influence of viscous force there, while it is prevailing in the central region where the wall influence is weak. Contrary in an electroosmotic flow, fluid flow is dragged by the thin ionic mobile layer near the solid–liquid interface and flows rapidly in the wall region, however it may become suppressed and even reversed in the central region due to the lack of driving force there [1]. The evident distinction in driving mechanisms implies a significant difference in flow distribution between the two flows. To make an intuitive understanding, herein consider the flow distribution on the middle cross-section of the floc A, as shown in Fig. 3. The whole cross-section is segregated into 10×10 subsections, and these subsections are successively numbered from 0 to 99 (only parts of the numbers are shown in Fig. 3) for the sake of an easy reference.

Fig. 4 shows the flowrate distribution: the flowrate percentage in each subsection is represented by a solid column and a blank column for the pressure driven flow and the electroosmotic flow, respectively. Difference in flowrate distribution between the two flows is evidenced by the non-overlapping profiles of the columns. Some subsections are completely occupied by solid matrix, i.e., the black area in Fig. 3, so no fluid flows through these subsections, such as subsections No.26 and 37 in Fig. 4. In the central region of flow channel(s), such as subsections No. 11, 21, 31, 41, 81 and 84, flowrate is larger in the pressure driven flow however much smaller in the electroosmotic flow. On the other hand, in the boundary region, such as subsections No. 25, 35, 44, 62 and 66, flowrate is quiet weak in the pressure driven flow while significantly increases in the electroosmotic flow.

In Fig. 4, flow distribution of the electroosmotic flow generally seems more uniform than that of the pressure driven flow, since the flowrate in boundary regions is enhanced while that in the central regions is relatively reduced. In porous media with pores of various sizes, pressure driven flow tends to concentrated in some large pores [21], causing a quite inhomogeneous flow; however, electroosmotic flow prefers to pass through small pores as well as large ones due to the electroosmotic driving force in the boundary region, so has a more uniform flow distribution. To make a quantitative understanding on this, a flowrate distribution factor is defined as

$$\chi = \frac{\int_{A_c} (u_n - u_m)^2 dA}{u_m^2 A_c} \tag{8}$$

where A_c is the cross-section area, u_n the velocity in the flow direction. χ is zero for an ideally uniform flow and increases as the flow deviates further from the idea one. For a tubular Poiseuille flow, χ is 0.33.

The values of parameter χ for each floc and each type of flow are presented in the parentheses in Fig. 5. Pressure driven flow in floc C has the largest χ while electroosmotic flow in floc A has the smallest one, indicating flow distribution is the most inhomogeneous in the former while the most homogeneous in the latter. For each sample, χ has a smaller value in the electroosmotic flow than in the pressure driven flow, which verifies the previous observation

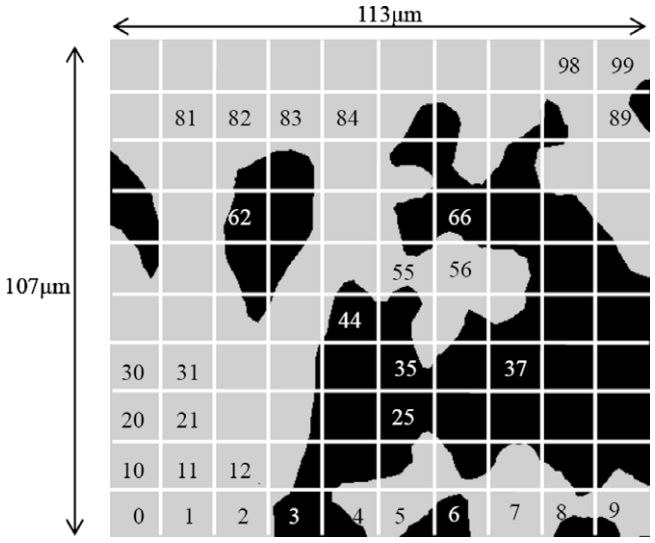

Fig. 3. Middle cross-section of floc sample A: pore in gray and solid in black.

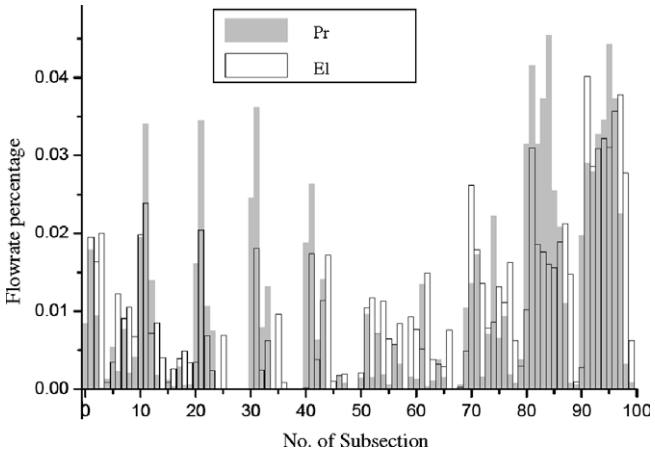

Fig. 4. Flowrate percentage in each subsection in Fig. 3: Pr – pressure driven flow; El – electroosmotic flow.

on Fig. 4 that electroosmotic flow has a more uniform flowrate distribution than pressure driven flow.

The flowrate accumulation curve also can give a clear vision on the flow distribution. Obtaining the accumulation curve needs to go through the following steps. First, the pore area in a specific cross-section is divided into many small areas and flowrate in each area is obtained; then these areas are sequentially numbered according to their flowrate from the largest to the smallest, which yields a sequence (*Seq*: $A_1, A_2, ..., A_i, ..., A_n$). Finally, the accumulative area A_a and flowrate Q_a are calculated as

$$A_a(i) = \int_1^i \mathrm{d}A_i, \quad Q_a(i) = \int_1^i \mathrm{d}Q_i \tag{9}$$

Since both A_a and Q_a are functions of the sequential number i, a direct relation holds as $Q_a = Q_a(A_a)$ which presents a curve in the Q_a–A_a plot. Q_a–A_a curve regresses into a linear line for an ideally uniform flow while becomes significantly convex for a non-uniform flow. Usually, a curve having a more rapid increasing rate at the beginning appears more convex, see Fig. 5. In this way, the uniformity of a flow can be explicitly reflected by the shape of the flowrate accumulation curve.

Fig. 5 shows the flow accumulation curves on the middle cross-sections of the three flocs for both the pressure driven and the electroosmotic flows. Please note that Q_a and A_a in Fig. 5 are normalized by the total flowrate Q_t and the total area A_t, respectively. For each floc sample, the curve of electroosmotic flow rises slower, or appears less convex, at the beginning than that of pressure driven flow, which indicates that electroosmotic flow has a more uniform flow distribution. This statement is accordant with the previous analyses. For each type of flow, the convexity sequence from small to large is the same, i.e., sample A is the smallest, sample B the medium, and sample C the largest, strongly indicating that in both types of flows the structure characteristics of flocs have important influence on the flow distribution.

Another notable phenomenon in Fig. 5 is that negative slop appears near (1, 1) on the curve for the electroosmotic flow of Floc C, indicating that reversed flow occurs on some areas in the cross-section. However, this phenomenon does not happen to the pressure driven flow in Floc C, implying that no reversed flow exists. In an electroosmotic flow, fluid is under strong influence of electrical force and flows forward near boundary, while is relatively easy to be reversed in the central region due to the lack of a strong driving force there. However, in a pressure driven flow fluid in both the boundary and central regions is under the intense driving of pressure gradient and therefore is hard to flow backward. This is why reversed flow is generally easy to happen in electroosmotic flow.

4.2. Pressure drop

The average pressure p_m on nine equally-spaced cross-sections, numbered successively from 0.1 to 0.9, are retrieved to show pressure variation along the flow direction inside flocs, as depicted in Fig. 6. Note that the inlet and outlet cross-sections are numbered as 0.0 and 1.0, respectively.

In pressure driven flows, the average pressure monotonically decreases along the flow direction in order to overcome the viscous resistance, while in electroosmotic flows where electrical force is the driving force to overcome the flow viscous force, pressure may not necessarily decrease. In this work, the calculation sets a zero pressure difference between the inlet and outlet in the electroosmotic flows in order to eliminate the influence of external pressure difference. This is why the pressure in electroosmotic flows varies around the horizontal line in Fig. 6.

Actually, pressure variation is still notable in electroosmotic flows. Taking the curve of the electroosmotic flow in Floc C as an example, on the 0.4 cross-section pressure gradient is negative to facilitate the flow, whereas on some other cross-sections, like the 0.2 cross-section, pressure gradient is positive to suppress the flow. This phenomenon is very common to the electroosmotic flows in this work and is expected to be caused by the structural properties of flocs. A simple model is proposed to explain the physical significance, as shown in Fig. 7.

A floc can be treated as composed of several porous sections serially connected along the flow direction. Each porous section is mechanically equivalent to a porous electroosmotic pump (EMP), so the floc is virtually assembled by several EMPs in series, e.g., 3 EMPs in Fig. 7. Each EMP in a series has its distinctive internal porous structure so its electroosmotic pumping capacity is different from that of other EMPs in the series. Some EMPs have sufficient and large pumping capacities and encounter with positive pressure gradient (positive pressure gradient suppresses flow) in the EMP series, while others have relatively weak pumping capacities and come up with negative pressure gradient (negative pressure gradient enhances flow). In this way, a unique flowrate can be met by all EMPs in the series. Fig. 7 gives some examples of different combinations of EMPs, which shows a determinant role of the local electroosmotic pumping capacity on the pressure variation along the flow direction.

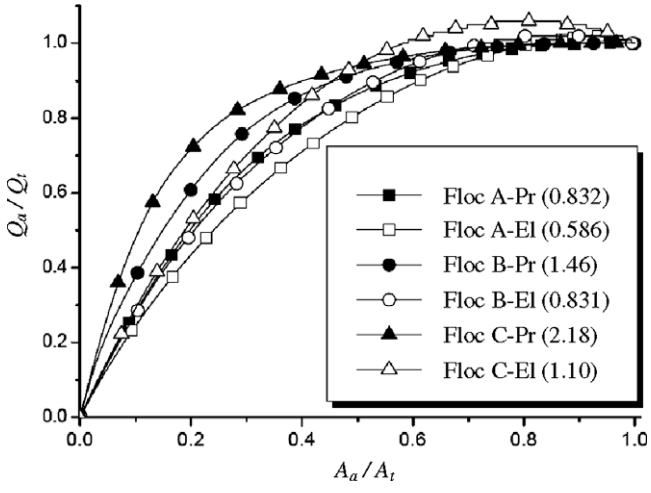

Fig. 5. Accumulation of flowrate: Pr – pressure driven flow; El – electroosmotic flow.

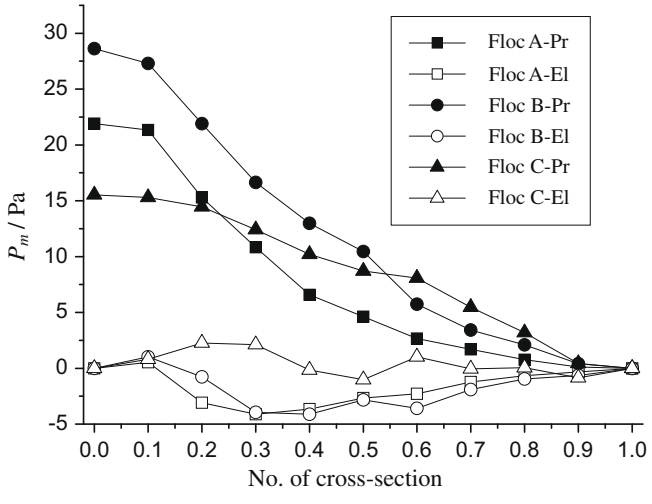

Fig. 6. Pressure change along the flow direction: Pr – pressure driven flow; El – electroosmotic flow.

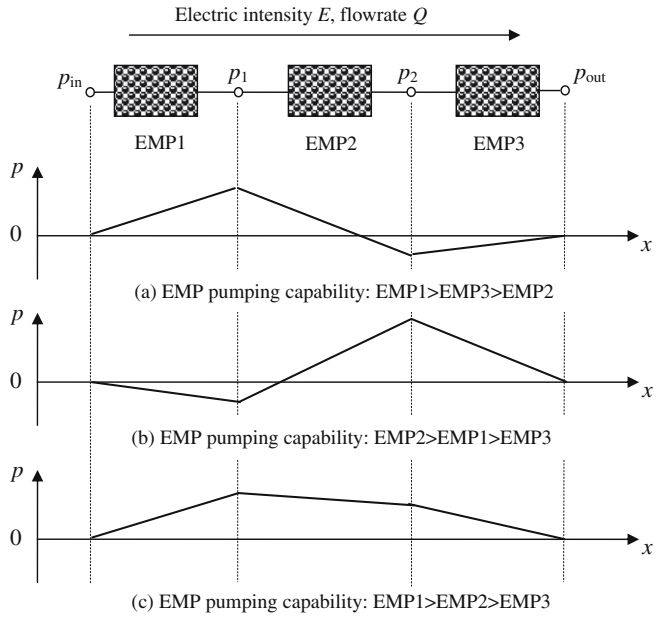

Fig. 7. EMPs in series.

4.3. Permeability

Permeability is a crucial parameter in determining sludge dewatering process. This part discusses the influence of Reynolds number and floc size on the permeability of electroosmotic and pressure driven flows.

4.3.1. Influence of Reynolds number

The permeability for a pressure driven flow in porous media is defined as

$$K_p = -\frac{\mu u_m}{\nabla_{flow} p} \tag{10}$$

where ∇_{flow} is gradient along flow direction. Similarly, the permeability for the electroosmotic flow can be defined as

$$K_{EM} = \frac{\mu u_m}{E_{flow}} \tag{11}$$

where E_{flow} is electric intensity along the flow direction which acts as the driving force in the electroosmotic flow.

Due to the difference in the driving mechanism, the unit of K_{EM} is Coulomb per meter (C/m) and is different from that of K_p, i.e., square meter (m^2). Table 2 gives the values of K_{EM} and K_p at different Reynolds numbers for all the three flocs. Note that the two different types of permeabilities have the same order, i.e., 10^{-12} in their values, which happens coincidently only as the zeta potential is of tens of micro-volts in this calculation. If the zeta potential is about several volts, K_{EM} will be two orders higher than K_p. A floc with high K_p may not be meant to have a high K_{EM}. For instance, at a *Re* of 0.01 Floc C has the largest K_p while its K_{EM} is not the largest. This is because of the different driving mechanisms between the two types of flows.

It is also observed that both K_{EM} and K_p decrease in each floc sample as *Re* increases. At a high Reynolds value, the inertial force becomes relatively important compared with the viscous force. The increased inertial force tends to augment the flow resistance in porous structures [19]. Consequently, the floc permeability declines for both cases. Fig. 8 shows a more explicit image on the decrease of permeability with increased Reynolds number, and both K_{EM} and K_p are normalized by their respective values at *Re* of 0.01.

Very clearly, permeability for both flows in all the flocs holds on a constant level at the low Reynolds number range and declines obviously as *Re* exceeds 10. The change of permeability with Reynolds number is closely dependent on the variation of flow distribution [20]. When the inertial force is weak, flow distributions have almost the same profiles so that the permeability is nearly unchanged. Whereas, as the inertial force becomes significant at high Reynolds numbers, flow distribution greatly alters, and consequently permeability decreases. In a specific floc, K_p decreases faster than K_{EM} doses, as shown in Fig. 8. For example, at *Re* = 500 in Floc C the deduction of K_p is 47% compared with that at *Re* = 100, while K_{EM} only reduced by 28%. The less deduction of K_{EM} implies that an electroosmotic flow can suppress the negative effect of the inertial force on flow in a more efficiently way than a pressure driven flow does. The intrinsic cause of this phenomenon concerns the fact that the electroosmotic flow has a more uniform flowrate distribution. More detailed discussions can be found in [19].

4.3.2. Influence of floc size

Reasonably, the driving mechanisms are expected to cause different size influence on permeability of a floc for the two flows. The following discussion is focused on the low Reynolds flows, i.e., $Re \ll 1$, so the influence of the inertial force can be safely neglected.

(a) *Size influence on K_p*

Ignoring inertial term in Eq. (2) yields

$$\nabla p' = \frac{1}{Re}\nabla^2 \vec{u}' \tag{12}$$

Introducing $P' = Re \cdot p'$ to Eq. (12), or

$$\nabla P' = \nabla^2 \vec{u}' \tag{13}$$

The corresponding boundary conditions for Eq. (13) on the floc surface and at the inlet are specified by Eqs. (7a) and (7b), respectively, and at the outlet

$$P' = 0 \tag{14}$$

The expression of K_p in Eq. (10) can be rewritten as

$$K_p = \frac{\mu u_m}{\nabla_{flow} p} = \frac{l_m^2}{\nabla'_{flow} P} \tag{15}$$

For similar structures of various sizes, Eq. (13) has a uniquely determined solution, and the denominator in Eq. (15) is constant. So K_p is linearly proportional to square of the floc size or $l_m{}^2$.

(b) *Size influence on K_{EM}*

At a low Reynolds number, electroosmotic flow in flocs can also be described by Eq. (13) with the boundary conditions as shown in Eqs. 4a–c, except that *p*' is replaced with *P*'. The expression of K_{EM} in Eq. (11) can be rewritten as

$$K_{EM} = \frac{\mu u_m}{E_{flow}} = -\varepsilon\varepsilon_0\zeta_w u'_m \tag{16}$$

where u'_m is the dimensionless average velocity. Since the solution of Eq. (13) is determined no matter what the characteristic length l_m is, u'_m is fixed as a constant for all structures of a similar geometry with different sizes. Thus, K_{EM} is independent upon l_m.

(c) *Comparisons*

Eqs. (15) and (16) tell the different dependences of K_p and K_{EM} on the floc size, respectively. To further verify these relations, per-

Table 2
Permeabilities at different Reynolds numbers.

Re*	Floc A		Floc B		Floc C	
	K_p/m^2	K_{EM}/C/m	K_p/m^2	K_{EM}/C/m	K_p/m^2	K_{EM}/C/m
0.01	4.54×10^{-12}	3.05×10^{-12}	3.34×10^{-12}	2.55×10^{-12}	5.46×10^{-12}	3.03×10^{-12}
0.1	4.55×10^{-12}	3.05×10^{-12}	3.35×10^{-12}	2.54×10^{-12}	5.46×10^{-12}	3.03×10^{-12}
1	4.54×10^{-12}	3.05×10^{-12}	3.34×10^{-12}	2.54×10^{-12}	5.40×10^{-12}	3.02×10^{-12}
10	4.36×10^{-12}	3.01×10^{-12}	3.16×10^{-12}	2.49×10^{-12}	4.73×10^{-12}	2.92×10^{-12}
100	2.99×10^{-12}	2.49×10^{-12}	2.02×10^{-12}	1.91×10^{-12}	2.73×10^{-12}	2.25×10^{-12}
500	1.73×10^{-12}	1.67×10^{-12}	1.12×10^{-12}	1.19×10^{-12}	1.53×10^{-12}	1.43×10^{-12}

* Reynolds numbers for both flows are defined by the mean flow velocity u_m to make sure that K_{EM} and K_p are compared at a same flowrate.

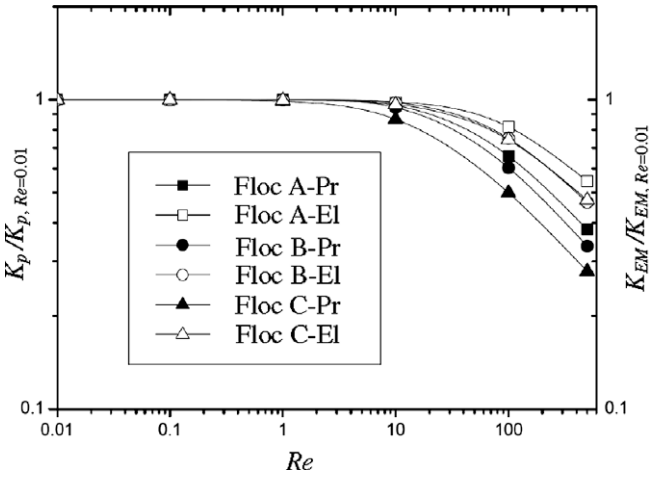

Fig. 8. Change of permeability with Reynolds number: Pr – pressure driven flow; El – electroosmotic flow.

meability of the floc A at different scales is simulated. This is done by first rescaling the structure of floc A to different sizes, i.e., creating a series of similar floc structures but with different sizes, and then numerically calculating K_p and K_{EM} for the floc at each size. As shown in Fig. 9, the numerical simulations indicate that the dependences of K_p and K_{EM} on the floc size very well accord with the theoretical predictions by Eqs. (15) and (16). The regression factors of both lines are above 0.9999. The K_{EM} is independent of floc size while K_p is linearly proportional to the floc size in the log–log plot, and has a slope of 1.99, very close to the value of 2 as predicted by Eq. (15).

Since sludge flocs formed during the same process can be treated as fractals [22–24], which means that they have similar structures in spite of their different sizes, K_p of sludge flocs should comply with Eq. (15) and is proportional to the square of floc size. This indicates that the pressure driven flow in small flocs has a small permeability and therefore becomes difficult. On the contrary, as shown by Eq. (16), the permeability of electroosmotic flow does not deteriorate with the decrease of floc size, which endows the electroosmotic flow a prominent capability to propel a flow in small-sized flocs, say below 100 μm. This feature is especially useful when applying electroosmotic flow to dewatering sludge which is aggregated by flocs.

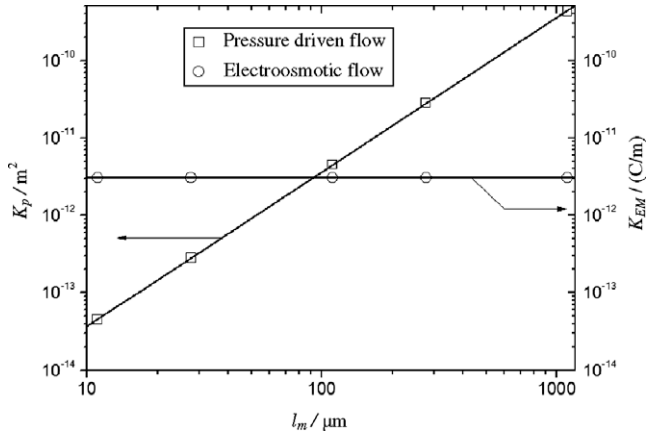

Fig. 9. Effect of floc size on permeability: circles and squares – numerical data; solid lines – linear regression.

5. Conclusions

In sludge flocs, electroosmotic flow has a more uniform flowrate distribution among pores of different sizes. It is this flow property that electroosmotic flow has a strong capability to resist the effect of the inertial force so as to slow down the reduction rate of permeability at high Reynolds numbers.

Pressure oscillates along the flow direction in electroosmotic flow, unlike the monotony of decline in pressure driven flow. This unique variation of pressure in the electroosmotic flow was explored to be caused by the change of local electroosmotic pumping capability in flocs.

When Reynolds number is low and the inertial force of flow is negligible, floc size does not influence permeability in electroosmotic flow, not like the case in pressure driven flow where permeability decreases with floc size.

Acknowledgement

This research is currently supported by the National Science Foundation of China (Contract No. 50636030).

References

[1] Z. Yang, X.F. Peng, B.X. Wang, Fully developed electroosmotically and hydrodynamically induced convection between two parallel plates, Numer. Heat Transfer A 50 (10) (2006) 905–926.
[2] M.H. Oddy, J.G. Santiago, J.C. Mikkelsen, Electrokinetic Instability Micromixing, Anal. Chem. 73 (2001) 5822–5832.
[3] W.T. Hung, I.L. Chang, W.W. Lin, Unidirectional freezing of waste-activated sludges: effects of freezing speed, Environ. Sci. Technol. 30 (1996) 2391–2396.
[4] D.J. Lee, Y.H. Hsu, Fast freeze/thaw treatment on excess activated sludge: floc structure and sludge dewaterability, Environ. Sci. Technol. 28 (1994) 1444–1449.
[5] M.H. M Raats, A.J.G. Diemen, J. Laven, Full scale electrokinetic dewatering of waste sludge, Colloid Surf. A: Pysicochem. Eng. Aspects 210 (2002) 231–241.
[6] C. Yuan, C.H. Weng, Sludge dewatering by electrokinetic technique: effect of processing time and potential gradient, Adv. Environ. Res. 7 (3) (2003) 727–732.
[7] J.X. Zhou, Z. Liu, P. She, Water removal from sludge in a horizontal electric field, Drying Technol. 19 (3–4) (2001) 627–638.
[8] S. Laursen, J. Birgerjensen, Electroosmosis in filter cakes of activated-sludge, Water Res. 27 (5) (1993) 777–783.
[9] S. Kondoh, M. Hiraoka, Commercialization of pressurized electroosmotic dehydrator (PED), Water Sci. Technol. 22 (12) (1990) 259–268.
[10] H. Yoshida, Practical aspects of dewatering enhanced by electro-osmosis, Drying Technol. 11 (4) (1993) 787–814.

[11] H. Yoshida, K. Kitajyo, M. Nakayama, Electroosmotic dewatering under A.C. electric field with periodic reversals of electrode polarity, Drying Technol. 17 (3) (1999) 539–554.
[12] K. Weber, W. Stahl, Improvement of filtration kinetics by pressure electrofiltration, Separ. Purif. Technol. 26 (1) (2002) 69–80.
[13] N. Otsu, A threshold selection method from gray-level histogram, IEEE Trans. Syst. Man Cyb. 9 (1) (1979) 62–66.
[14] C.P. Chu, D.J. Lee, Advective flow in a sludge floc, J. Colloid Interface Sci. 277 (2) (2004) 387–395.
[15] C.P. Chu, D.J. Lee, Multiscale structure of biological flocs, Chem. Eng. Sci. 59 (8–9) (2004) 1875–1883.
[16] Z. Yang, X.F. Peng, C.P. Chu, D.J. Lee, A. Su, Sedimentation of permeable floc, Drying Technol. 24 (2006) 1277–1282.
[17] Z. Yang, X.F. Peng, C.P. Chu, D.J. Lee, Image processing and geometric parameters extracted from sliced image of porous biomaterial, Adv. Powder Technol. 18 (2) (2007) 187–213.
[18] Z. Yang, X.F. Peng, D.J. Lee, S. Ay, Advective flow in spherical floc, Colloid Interface Sci. 308 (2007) 451–459.
[19] Z. Yang, X.F. Peng, B.X. Wang, Numerical investigation on electroosmotic transport in porous media, in: Proceedings of the ASME Summer Heat Transfer Conference, vol. 3, San Francisco CA, 2005, pp. 703–709.
[20] Z. Yang, X.F. Peng, D.J. Lee, A. Su, Reynolds number-dependent permeability of wastewater sludge flocs, J. Chinese Inst. Chem. Eng. 38 (2007) 135–141.
[21] Z. Yang, X.F. Peng, M.Y. Chen, D.J. Lee, J.Y. La, Intra-layer flow in fouling layer on membranes, J. Membrane Sci. 287 (2007) 280–286.
[22] N. Tambo, Y. Watanabe, Physical characteristics of floc – I. The floc density function and aluminum floc, Water Res. 13 (1979) 409–419.
[23] D.H. Li, J.J. Ganczarczyk, Fractal geometry of particle aggregates generated in water and wastewater treatment processes, Environ. Sci. Technol. 23 (1989) 1385–1389.
[24] D.J. Lee, Floc structure and bound water content in excess activated sludges, J Chinese Inst. Chem. Eng. 25 (1994) 201–207.